PRAMANA — journal of physics

Vol. 84, No. 6
June 2015
pp. 999–1009

Correlation effects driven by reduced dimensionality in magnetic surface alloys

U MANJU
CSIR-Institute of Minerals and Materials Technology, Sachivalaya Marg, Bhubaneswar 751 013, India
E-mail: manju@immt.res.in, manju.unnikrishnan@gmail.com

DOI: 10.1007/s12043-015-0997-5; ***e*Publication:** 2 June 2015

Abstract. The evolution of electronic properties and correlation effects in manganese-based two-dimensional magnetic surface alloys are discussed. Enhanced correlations resulting from the reduced dimensionality of the surface alloys lead to the modification of the core level and valence band electronic structures resulting in the appearance of distinct satellite features. Apart from this, surface alloying-induced strong modifications in the substrate surface states arising from charge reorganization and electron transfer to the surface states as well as band-gap openings are also discussed.

Keywords. Magnetic surface alloys; electronic structure; surface reconstructions; correlation satellites; charge reorganization.

PACS Nos 79.60.Dp; 73.20.At

1. Introduction

Magnetically stabilized ordered surface alloys, consisting of a non-magnetic metallic surface where the atoms with a large magnetic moment arrange in ordered superstructures, have attracted increasing attention due to the possibility of tailoring their properties for potential applications in data storage and spin injection devices [1–3]. Surprisingly, such surface alloy formations are observed even for some metal–metal combinations which are practically immiscible in the bulk. The stability of these surface alloys results from the presence of a large magnetic moment of the constituent atoms as shown by *ab-initio* electronic structure calculations. Among these systems, Mn and related compounds are of particular interest due to the high magnetic moment (5 μ_B) expected for Mn according to Hund's rules. For instance, in the $c(2\times2)$ Mn/Cu(1 0 0), $c(2\times2)$ Mn/Ni(1 0 0) and $c(2\times2)$ Mn/Cu(1 1 0) surface alloys, Mn magnetic moment reaches 3.75 μ_B, 3.5 μ_B and 3.82 μ_B, respectively [4–7]. Due to the nearly half-filled $3d$ shell, the low-coordinated Mn has a stable high-spin ground state, whereas an itinerant low-spin ground state is formed in Mn metal, thereby making Mn an ideal material to study the interplay between hybridization and magnetic ordering.

While Mn and Cu do not form stable bulk compounds, the $c(2\times2)$ surface compound turns out to be a very stable two-dimensional system. Structural investigations suggest that these alloys are characterized by a considerable atomic corrugation in the surface layer during alloy formation. For example, in the case of $c(2\times2)$ Mn/Cu(1 1 0) surface alloys, the Mn atoms buckle outward and the Cu atoms inward with a total buckling amplitude of 0.22 Å (17.2% of the ideal interlayer distance in Cu(1 1 0)) [7]. The stability of these two-dimensional (2D) systems is due to the large gain in the magnetic energy associated with an outward buckling of the Mn atoms [4,8,9]. It was further suggested that the buckling reverts the coupling between the Mn magnetic moments from antiparallel to parallel resulting in a long-range ferromagnetic order. A large Mn magnetic moment of 3.82 μ_B was predicted and proposed to be the origin of the large electronic structure modifications that lead to the change in work function [7]. The close relationship between the atomic structure and the magnetic properties has made Mn–Cu surface alloys one of the most investigated two-dimensional surface alloy systems.

Electronic and magnetic structures of transition metal atoms, when arranged in lower dimensions, forming ultrathin films and surface alloys, get strongly modified when compared to their bulk counterparts because the surface has a different coordination number and chemical environment as compared to the bulk. The wave functions have smaller overlaps leading to a reduction in the electronic bandwidth giving rise to an enhancement of the exchange splitting [10–12]. Here the d electrons exhibit much stronger correlation which could lead to strongly enhanced magnetic moments. The reduction of the crystal field at the surfaces as well as the narrowing of the d bands and the enhancement of the density-of-states at the Fermi level can modify the surface magnetic properties making them considerably different from the bulk magnetism [3]. For example, Mn/Ag(1 0 0) shows a magnetic moment as large as 4 μ_B, close to Hund's rule ground-state value as opposed to the itinerant low-spin ground-state formed in Mn metal [13]. The understanding of the surface magnetic properties and their origin are of utmost importance for technological applications involving phenomena such as giant magnetoresistance, oscillatory interlayer coupling, spin injection and high-density storage devices. Lowering of bandwidth also induces increased localization of the electrons and electron correlation effects can be strongly enhanced, as revealed by the appearance of satellite structures in the core level or more rarely in the valence band photoemission spectra. The origin and thickness dependence of these satellite structures in the Mn $2p$ core level spectra from Mn metal films grown on Al substrates have been reported previously where intra-atomic multiplet effect associated with Mn atoms with large local moment plays a significant role [14]. Hence understanding the electronic correlations arising from the reduced dimensionality become increasingly important. Here we look at the modifications of the electronic structure of various Mn-based ordered magnetic surface alloys arising from enhanced electronic correlations due to surface alloying.

2. Sample preparation and characterization

Surface alloys are generally prepared *in situ* by chemical vapour deposition technique. The surface of the metallic substrate is first prepared by repeated cycles of Ar^+ sputtering, followed by annealing at appropriate temperatures. The cleanliness of the surface is monitored by the appearance of sharp low energy electron diffraction (LEED) patterns or by

the absence of the core level C 1*s* and O 2*p* signals in the X-ray photoemission spectra or the respective signals in the Auger electron spectra. The second constituent of the surface alloy is subsequently deposited by keeping the substrate at appropriate temperatures and monitoring the rate of deposition using a quartz thickness monitor so as to carefully follow the formation of various ordered superstructures during the alloy formation. For example, for preparing Mn/Cu(1 1 0) surface alloy, a clean Cu(1 1 0) surface was prepared by repeated cycles of Ar^+ ion sputtering and annealing to 750 K [15]. The clean surface shows sharp $p(1\times1)$ LEED pattern as shown in figure 1a. Manganese was deposited *in situ*, using an electron beam evaporation source, by keeping the Cu(1 1 0) substrate at room temperature. New superstructures start appearing in the LEED pattern after Mn deposition. The sub monolayer coverages lead to the formation of $c(2\times2)$ superstructure characterized initially by faint and very diffused spots which gain sharpness and intensity with increasing coverages. A maximum order is reached at 0.5 monolayer (ML) as shown in figure 1b. A schematic of the $c(2\times2)$ ordered superstructure showing the atomic corrugation is shown in figure 1c where Mn atoms are embedded in the top surface layer of Cu(1 1 0) substituting every second Cu atom forming a checker-board-like structure with the remaining Cu surface atoms. Beyond 0.5 ML Mn, $c(2\times2)$ spots get broader and decrease in intensity and vanish between 1.0 and 1.5 ML Mn. In this range, both $c(2\times2)$ phase and a higher (16×1) superstructure phase coexist. Beyond 2 ML, pure (16×1) phase remains [15]. Spectroscopic measurements on Mn/Cu(1 1 0) discussed here were performed at the APE-INFM beamline at the Elettra Synchrotron Light Source, Italy, where on the very same sample surfaces the electronic band dispersions as well as the core level photoemission and absorption spectra were acquired. All angle-resolved photoemission spectroscopy (ARPES) measurements were performed using linearly polarized

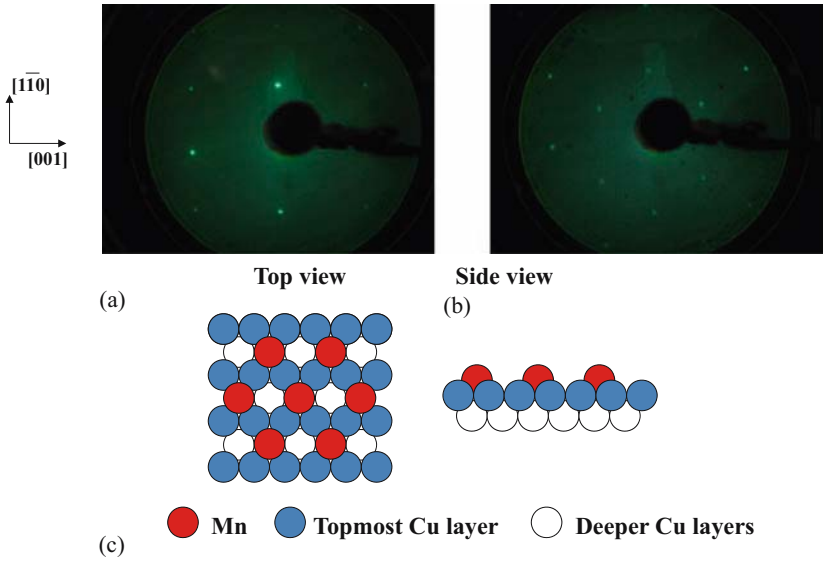

Figure 1. Low-energy electron diffraction patterns of (**a**) clean Cu(1 1 0) and (**b**) $c(2\times2)$ Mn/Cu(1 1 0). (**c**) Schematic of $c(2\times2)$ ordered superstructure showing atomic corrugation.

light and recorded using Scienta SES2002 electron energy analyser. X-ray photoemission spectroscopy (XPS) measurements were recorded using an Omicron EA125 hemispherical electron energy analyser whereas the Mn $L_{2,3}$ X-ray absorption edges were recorded by the total electron yield method. Valence band photoemission spectra from $c(2\times2)$ CuMn/Cu(1 0 0)
systems discussed here were measured at the TGM 1 beamline for linearly polarized synchrotron light at BESSY, Germany [12].

3. Correlation effects

Enhanced electron correlation effects and localization lead to the appearance of additional structures in the core level photoemission spectra, the so-called correlation satellites. Mn $2p$ core level photoemission spectra acquired from Mn/Cu(1 1 0) surface alloy for 0.125 ML, 0.5 ML and 5 ML Mn depositions are shown in figure 2. The spectra essentially consist of two main peaks appearing at ∼641.6 eV and ∼651.6 eV binding energy positions corresponding to the spin-orbit split Mn $2p_{3/2}$ and $2p_{1/2}$ states, along with two pronounced shoulders appearing at higher binding energies. The intensity of the shoulders is almost similar for 0.125 ML and 0.5 ML depositions, whereas they practically vanish for the 5 ML Mn coverage where the spectral features resemble that of bulk Mn. These satellite features are the manifestations of enhanced correlations present in Mn/Cu(1 1 0) surface alloy which originate from the reduced Mn–Mn coordination in the $c(2\times2)$ struc-

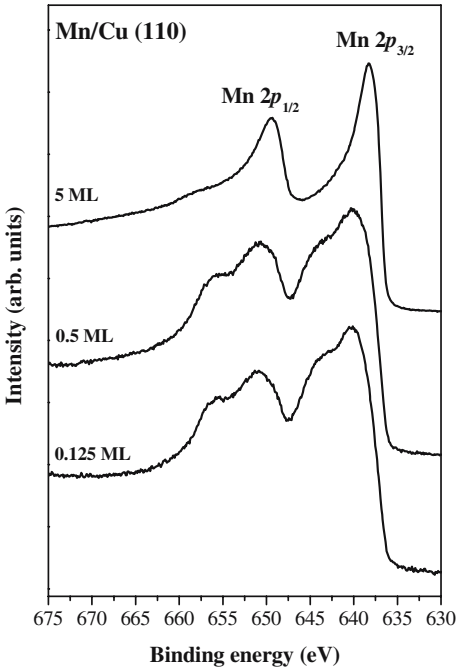

Figure 2. Mn $2p$ core-level photoemission spectra of 0.125, 0.5 and 5 ML Mn on Cu(1 1 0) substrate.

ture. As discussed previously in this checker-board-like structure, ideally no Mn–Mn next-neighbour pairs exist, and hence the overlap of the Mn 3*d*-derived wave functions and the corresponding 3*d* bandwidth, W, are reduced considerably. In contrast to an fcc bulk site with 12 next nearest neighbours, the Mn in the surface alloy has only eight neighbours placed further apart. Consequently, there is a reduction in the electronic screening, due to which the Coulomb interaction energy U increases and so the U/W ratio also increases. Almost equal intensities of the satellite features for 0.125 ML and 0.5 ML suggest that the ordering of Mn atoms into the $c(2\times2)$ structure starts even for small Mn depositions. Beyond 0.5 ML Mn coverage, each Mn atom starts seeing other Mn atoms in its neighbourhood leading to an increase in the Mn 3*d*–3*d* interactions and decrease in correlations, thereby reducing the intensity of the satellite features which eventually vanishes for higher Mn coverages. The Mn 2*p* main peak at lower binding energy could be assigned to the well-screened state described as $2p^5 3d^6 L^{-1}$ and the satellite peaks at higher binding energies to the poorly screened state of $2p^5 3d^5$, where L^{-1} denotes the ligand hole of the surrounding Cu 3*d* and Mn 3*d* states. It may also be noted that the average satellite-to-main peak energy separations for $2p_{1/2}$ and $2p_{3/2}$ states are 5 eV and 3.5 eV, respectively, arising from the atomic multiplet effects causing an apparent spin-orbit splitting that is greater for $2p^5 3d^5$ than for $2p^5 3d^6$ final states, leading to $\sim$1 eV larger main line splitting for the $2p_{1/2}$ than for the $2p_{3/2}$ lines [13,34].

By arranging Mn atoms in the two-dimensional alloy $c(2\times2)$ CuMn/Cu(1 0 0), correlation effects are enhanced to such an extent that distinct satellite structures unambiguously appear in their valence band photoemission spectra, as shown in figure 3 [12]. In the figure, apart from the Cu 3*d* emission peak appearing around 3–4 eV binding energy, which also contains Mn 3*d* majority-spin emission, Cu two-hole satellite contributes at 11.8 eV and 14.6 eV binding energies, Mn 3*p*3*d*3*d* Auger at fixed kinetic energy (noted by arrow marks) and the new satellite features arising from enhanced correlations at 8 eV and 9.6 eV binding energies. Various observations which are characteristics of correlation satellites could be noted here, viz. (a) the spectral features are well discernable below, at and above the Mn 3*p*–3*d* excitation threshold which is at 50 eV, (b) no dispersions with respect to photon energy or emission angles and (c) strong enhancement of intensity at the threshold. These features disappear with increasing Mn–Mn coordination. It has been shown that alloying of Mn with Cu cannot as such account for the creation of the valence band satellite features. The presence of the surface must be crucial because valence band satellite features are not observed in the photoemission studies of Mn impurities in bulk Cu, Ag and Au for various concentrations. This suggests that the increased localization in the surface alloy compared to an impurity site in the bulk is the origin of these additional features. Hence, one can conclude that correlation leading to the satellite must essentially be driven by the reduced dimensionality of the surface alloy compared to a bulk impurity site [12].

Surface alloying-induced enhanced correlations and satellite structures are also observed in the Mn 2*p* core level spectra of ultrathin Mn films on Cu(1 0 0) [6], Ni(1 1 0) [16] and Ag(1 0 0) [17] substrates. For Mn/Ag(1 0 0) the calculated spectra using the impurity model including full multiplet calculations could reproduce well the experimental spectra for a whole range of systems from Mn impurities in Ag to bulk Mn. The satellite structure in the ultrathin films is due to a final-state charge transfer process, mainly from Mn-*d* majority spin states on the neighbour atoms to the empty minority spin states of the emitter atom leading to $2p^5 3d^5$ and $2p^5 3d^6$ final states which are separated by 4–5 eV due to

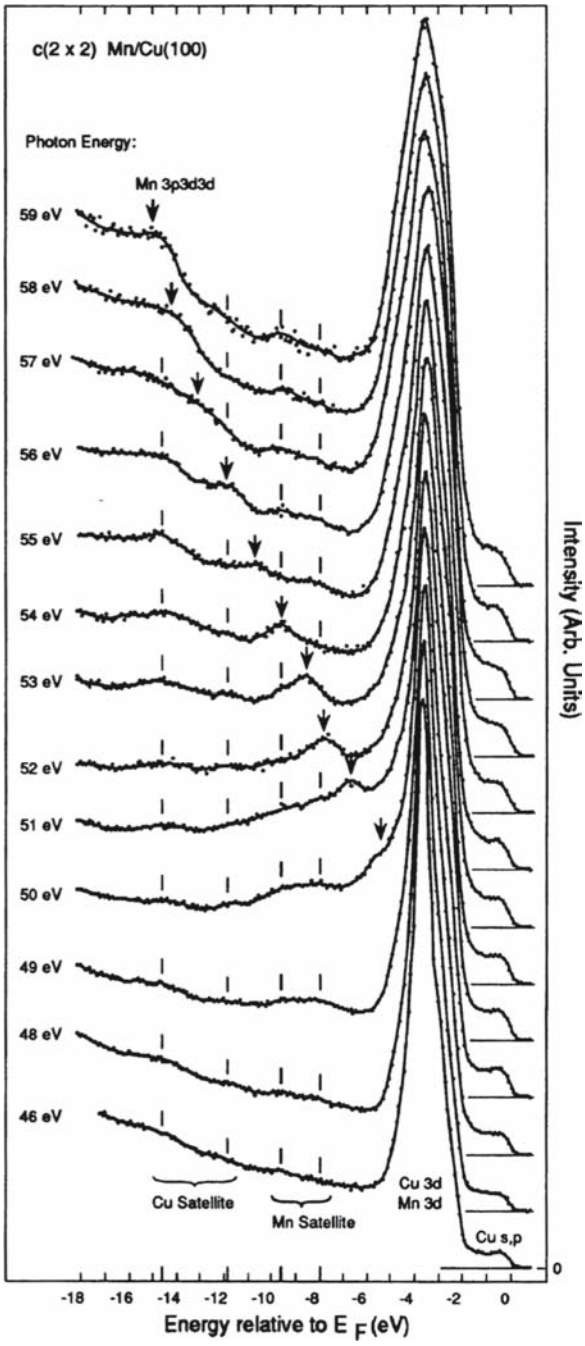

Figure 3. Photoemission spectra of the valence band range of $c(2\times2)$ Mn/Cu(1 0 0) for different photon energies across the Mn $3p$–$3d$ excitation threshold. Vertical bars mark satellite structures of Cu and Mn. The arrows mark Auger emission [12]. This figure is adopted from ref. [12].

the $2p$–$3d$ Coulomb interaction. The intensity ratio between these two types of final states essentially reflects the degree of Mn $3d$ hybridization. A progressive transfer of intensity from the poorly screened to the well-screened component with increasing coverage can be associated with increasing Mn $3d$ hybridization, faster $3d$ hoping and relevant charge fluctuations. While atomic multiplet effects are not directly visible as fine structure, they cause a small difference ($\sim$1 eV) between the apparent spin-orbit splitting of $2p^5 3d^5$ and $2p^5 3d^6$ final states [13].

Configuration interaction cluster calculations performed for $c(2\times2)$ Mn/Ni(110) and $c(2\times2)$ Mn/Cu(1 0 0) give the parameters $\Delta = 1.0$ eV, $U = 3.0$ eV and $dd\sigma = 1.2$ eV for the former and $\Delta = 1.5$ eV, $U = 3.0$ eV and $dd\sigma = 1.0$ eV for the latter, respectively where Δ is the Ni (Cu) $3d$ to Mn $3d$ charge transfer energy, U is the multiplet-averaged Mn $3d$–$3d$ interaction energy and $dd\sigma$ is the Slater–Koster parameter expressing the hopping matrix elements between Mn $3d$ and Ni (Cu) $3d$ orbitals [16]. A comparison of the extracted parameters for the above systems suggests that Δ and $dd\sigma$ vary slightly with the chemical environment (Ni and Cu, respectively), while U remains the same. The structural relaxations for $c(2\times2)$ Mn/Cu(1 0 0) and $c(2\times2)$ Mn/Ni(1 0 0) have been found to be very similar to each other, so it is for $c(2\times2)$ Mn/Cu(110) and $c(2\times2)$ Mn/Ni(110), suggesting that similar parameters could be extended to these systems as well where $\Delta < U$. This suggests that the main peak at the lower binding energy appearing in the Mn $2p$ spectra of the above systems are dominated by $2p^5 3d^6 L^{-1}$ and the satellite peaks at higher binding energies by $2p^5 3d^5$ as discussed previously. $\Delta \ll U$ also suggests that these surface alloys can be characterized as charge-transfer compounds, where in practice, the metallic conductivity of the systems will be provided by the Ni/Cu substrates [16,18].

X-ray absorption spectroscopy (XAS) is a very sensitive tool to probe the effects of $3d$ orbital hybridization in the ground state. The Mn $L_{2,3}$ edge XAS spectra of Mn/Cu(1 1 0) surface alloy for various Mn concentrations are shown in figure 4. Here also, apart from the two main absorption edges corresponding to the spin-orbit split components L_3 and L_2 that represent transitions into Mn $3d$ states that produce $2p_{3/2}$ and $2p_{1/2}$ core holes, additional fine structures are observed for 0.125 ML and 0.5 ML Mn coverages. These well-resolved multiplet structures, appearing as shoulders at $\sim$1 eV and $\sim$3 eV higher energy of the L_3 peak and a doublet peak structure of the L_2 component, are characteristic of an atomic-like $3d^5$ ground state [15,21]. Similar to the case of Mn $2p$ core level photoemission spectra, here also the satellite features vanish for 5 ML Mn coverage here. The line shape of the 5 ML coverage without any fine structures, in sharp contrast to the submonolayer coverage, is characteristic of the itinerant Mn $3d$ electrons. Hence a crossover from localized to itinerant $3d$ electron behaviour with increasing Mn coordination is observed, thereby reproducing the inferences from the core level photoemission spectra, confirming the role of electron correlations in dictating the electronic structure of this surface alloy. Similar behaviour has also been observed for $c(2\times2)$ Mn/Cu(1 0 0), $c(2\times2)$ Mn/Ni(1 0 0) [8,19] and $c(2\times2)$ Mn/Ag(1 0 0) [20] surface alloys and submonolayers of Mn on Fe(1 0 0) [21] substrates. For Mn films on Ni and Fe substrates, the electron correlation effects in a localized ground state with a nearly half-filled $3d$ shell were found to cause antiferromagnetic alignment between the substrate and the overlayer, which eventually switches to ferromagnetic order for an itinerant system.

4. Charge transfer effects

Apart from the correlation satellites, surface alloying also induces other important modifications in the valence band structures. For example, near-valence band spectra acquired using angle-resolved photoemission spectroscopy (ARPES) from the $\bar{Y}$ symmetry point for clean Cu(1 1 0) and Mn/Cu(1 1 0) surface alloys with increasing Mn content are shown in figure 5. The well-known Shockley surface state (SS) band of clean Cu(1 1 0) with a binding energy minimum at ∼0.49 eV is shown in figure 5a. Upon alloying, with Mn deposition, the binding energy minimum shifts towards higher binding energies and the diameter of the SS Fermi contour increases (figures 5b and 5c). This suggests an increase in the number of charge carriers occupying the surface state. It is well known that several mechanisms contribute to the modification of the surface states like Pauli repulsion [22,23], mixing and hybridization of electronic states [24–26], charge transfer [27,28], polarization [29,30] and surface relaxation [31,32]. Here, Mn-induced charge redistribution in the Cu surface layer is proposed. The structural investigation of Mn/Cu(1 1 0) surface alloy suggests that the Mn atoms induce a strong surface corrugation with total inward/outward Cu/Mn relaxation which might cause local charge transfer from the bulk to surface states. Along with the increase in SS Fermi contour, apparent change in the left–right asymmetry (with respect to $\bar{Y}$ symmetry point) of the SS intensity with increasing Mn coverage can also be noted with the implication that the p component of the sp originating Cu(1 1 0) Shockley surface state (which is linked to the transitions to d final states) changes due to hybridization with other symmetry components that 'spill in' new charge in the SS [15,33].

Besides the modifications at the $\bar{Y}$ symmetry point, new Mn-induced surface bands are identified at the $\bar{X}$ symmetry point of the surface Brillouin zone as shown in figure 6. Two-dimensional character of the bands has been confirmed from their nondispersive nature with varying photon energies, confirming that these bands arise from surface alloying. The bands gain in sharpness and intensity, while remaining at the same k point and same

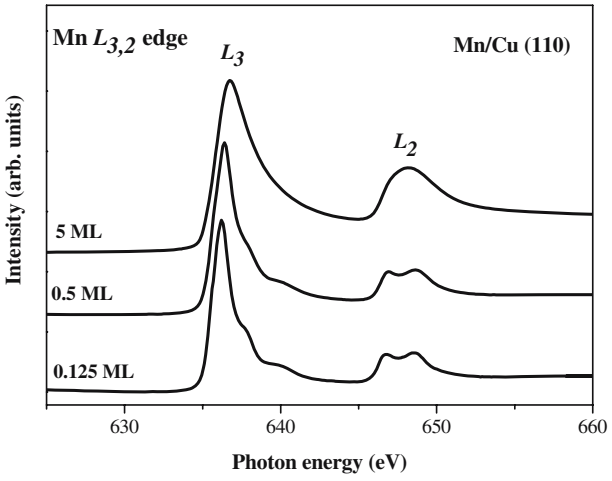

Figure 4. Mn $L_{2,3}$ X-ray absorption spectra of 0.125, 0.5 and 5 ML Mn on Cu(1 1 0) substrate.

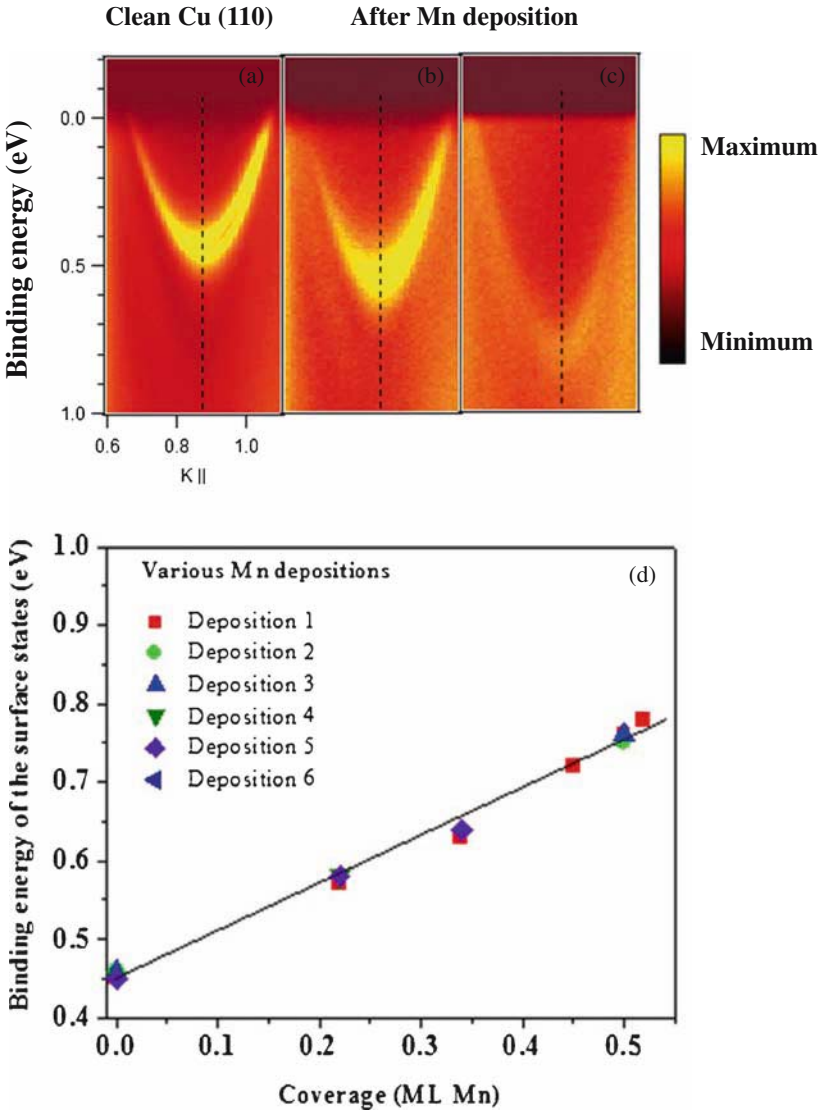

Figure 5. Shockley surface state around the $\bar{Y}$ symmetry point of the surface Brillouin zone for (**a**) clean Cu(1 1 0) and its evolution with increasing Mn concentration (**b**)–(**c**). The position of $\bar{Y}$ symmetry point is indicated by black dashed lines. (**d**) Shift in binding energy position of the Shockley SS for various Mn coverages.

binding energies, with increasing Mn concentration till the $c(2\times2)$ superstructure persists and vanishes when the (16×1) superstructure sets in for 2.5 ML Mn deposition suggesting that these bands are pertinent uniquely to the $c(2\times2)$ superstructure [15]. Also, these bands are backfolded with respect to $\bar{X}$ at ∼0.5 eV below E_F opening up a band gap in the occupied states. In the electronic structure of Pb–Cu alloys, buckling of the Pb layer leads to the repulsion of the bands at the crossing points leading to a band-gap opening, as this could

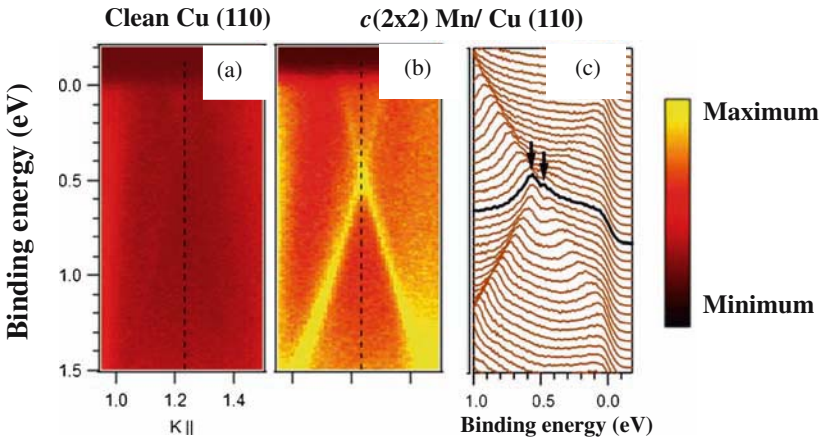

Figure 6. New electronic bands around the $\bar{X}$ symmetry point of the surface Brillouin zone arising from Mn deposition. (**a**) Clean Cu(1 1 0) showing that the intensity of the Cu bulk bands is almost completely suppressed. (**b**) 0.5 ML $c(2\times2)$ Mn/Cu(1 1 0) and (**c**) an expanded view of the energy distribution curves for 0.5 ML $c(2\times2)$ Mn/Cu(1 1 0) near the $\bar{X}$ point indicating a possible band gap of 100 meV.

provide a way for the adlayer to gain electronic energy, thereby compensating the enhanced elastic energy of the surface reconstruction [34,35]. Along the same lines this band-gap opening in Mn/Cu(1 1 0) is speculated to be a direct consequence of the large buckling of the Mn and Cu layers as observed from their structural studies.

Similar modifications in the valence band electronic structures have also been observed in the case of Mn/Cu(1 0 0) surface alloys where the Tamm-surface state at the $\bar{M}$ symmetry point of Cu(1 0 0) disappears completely upon the formation of the $c(2\times2)$ Mn/Cu(1 0 0) surface alloy and the electronic structure near the $\bar{X}$ symmetry point changes dramatically with the formation of new interface states [2,36]. One of these interface states has strong Shockley-type surface state characteristics and appear at a distinct binding energy position which shifts with increasing Mn coverage and work function changes. Theoretical analysis indicates a spin splitting of the surface state with the minority spin part unoccupied. The second interface state shows a stronger localization confirming a partly occupied Mn-derived spin minority band.

Acknowledgements

The author gratefully acknowledges the contributions from I Vobornik, G Rossi and D Topwal in the experiments on Mn/Cu(1 1 0) discussed here, which were performed at APE-INFM beamline at the Elettra Synchrotron Light Source, Italy and the financial support from the ICTP-TRIL Fellowship in this regard.

References

[1] F R Lucci, T J Lawton, A Pronschinske and E C H Sykes, *J. Phys. Chem. C* **118**, 3015 (2014)
[2] Bin Lu, Xiangdong Liu, Kan Nakatsuji, Takushi Iimori and Fumio Komori, *Phys. Rev. B* **76**, 245433 (2007)

[3] Y Huttel, C M Teodorescu, F Bertran and G Krill, *Phys. Rev. B* **64**, 094405 (2001)
[4] M Wuttig, Y Gauthier and S Blügel, *Phys. Rev. Lett.* **70**, 3619 (1993)
[5] M Eder, J Hafner and E G Moroni, *Phys. Rev. B* **61**, 11492 (2000)
[6] O Rader, W Gudat, C Carbone, E Vescovo, S Blügel, R Kläsges, W Eberhardt, M Wuttig, J Redinger and F J Himpsel, *Phys. Rev. B* **55**, 5404 (1997)
[7] Ch Ross, B Schirmer, M Wuttig, Y Gauthier, G Bihlmayer and S Blügel, *Phys. Rev. B* **57**, 2607 (1998)
[8] W L O' Brien and B P Tonner, *Phys. Rev. B* **51**, 617 (1995)
[9] M Wuttig, S Junghans, T Flores and S Blügel, *Phys. Rev. B* **53**, 7551 (1996)
[10] A J Fu, C L Freeman and T Oguchi, *Phys. Rev. B* **54**, 2700 (1985)
[11] S Blügel, *Phys. Rev. Lett.* **68**, 851 (1992)
[12] O Rader, E Vescovo, M Wuttig, D D Sarma, S Blügel, F J Himpsel, A Kimura, K S An, T Mizokawa, A Fujimori and C Carbone, *Europhys. Lett.* **39**, 429 (1997)
[13] P Krüger and A Kotani, *Phys. Rev. B* **68**, 035407 (2003)
[14] A K Shukla, P Krüger, R S Dhaka, D I Sayago, K Horn and S R Barman, *Phys. Rev. B* **75**, 235419 (2007)
[15] U Manju, D Topwal, G Rossi and I Vobornik, *Phys. Rev. B* **82**, 035442 (2010)
[16] O Rader, T Mizokawa, A Fujimori and A Kimura, *Phys. Rev. B* **64**, 165414 (2001)
[17] P Schieffer, C Krembel, M C Hanf and G Gewinner, *J. Electron Spectrosc. Relat. Phenom.* **104**, 127 (1999)
[18] U Manju, V P S Awana, H Kishan and D D Sarma, *Phys. Rev. B* **74**, 245106 (2006)
D D Sarma, *J. Solid State Chem.* **88**, 45 (1990)
Seva Nimkar, D D Sarma and H R Krishnamurthy, *Phys. Rev. B (Rapid Commun.)* **47**, 10927 (1993)
[19] W L O' Brien, J Zhang and B P Tonner, *J. Phys.-Cond.* **5**, L515 (1993)
[20] B T Thole, R D Cowan, G A Sawatzky, J Finck and J C Fuggle, *Phys. Rev. B* **31**, 6856 (1985)
[21] H A Dürr, G van der Laan, D Spanke, F U Hillebrecht and N B Brookes, *Phys. Rev. B* **56**, 8156 (1997)
[22] T Andreev, I Barke and H Hövel, *Phys. Rev. B* **70**, 205426 (2004)
[23] F Forster, S Hüfner and F Reinert, *J. Phys. Chem. B* **108**, 14692 (2004)
[24] A Tamai, A P Seitsonen, F Baumberger, M Hengsberger, Z-X Shen, T Greber and J Osterwalder, *Phys. Rev. B* **77**, 075134 (2008)
[25] A Ferretti, C Baldacchini, A Calzolari, R Di Felice, A Ruini, E Molinari and M G Betti, *Phys. Rev. Lett.* **99**, 046802 (2007)
[26] K Kanazawa, Y Sainoo, Y Konishi, S Yoshida, A Taninaka, A Okada, M Berthe, N Kobayashi, O Takeuchi and H Shigekawa, *J. Am. Chem. Soc.* **129**, 740 (2007)
[27] S A Lindgren and L Walldén, *Solid-State Commun.* **28**, 283 (1978)
[28] E Bertel, *Surf. Sci.* **331–333**, 1136 (1995)
[29] M Preuss, W G Schmidt and F Bechstedt, *Phys. Rev. Lett.* **94**, 236102 (2005)
[30] W G Schmidt, K Seino, M Preuss, A Hermann, F Ortmann and F Bechstedt, *Appl. Phys. A: Mater. Sci. Process. B* **85**, 387 (2006)
[31] I Vobornik, J Fujii, M Mulazzi, G Panaccione, M Hochstrasser and G Rossi, *Phys. Rev. B* **72**, 165424 (2005)
[32] I Vobornik, J Fujii, M Hochstrasser, D Krizmancic, C E Viol, G Panaccione, S Fabris, S Baroni and G Rossi, *Phys. Rev. Lett.* **99**, 166403 (2007)
[33] M Mulazzi, G Rossi, J Braun, J Minar, H Ebert, G Panaccione, I Vobornik and J Fujii, *Phys. Rev. B* **79**, 165421 (2009)
[34] S Müller, J E Prieto, C Rath, L Hammer, R Miranda and K Heinz, *J. Phys.: Condens. Matter* **13**, 1793 (2001)
[35] F Baumberger, A Tamai, M Muntwiler, T Greber and J Osterwalder, *Surf. Sci.* **532–535**, 82 (2003)
[36] F Schiller, S V Halilov and C Laubschat, *Phys. Rev. B* **65**, 184430 (2002)